Decoding Activation of ILC2 using Time-Dependent Cell-State Selection

Yumiko Tanaka
The University of Tokyo
Mai Yamagishi
The University of Tokyo
Yasutaka Motomura
Osaka University
Takashi Kamatani
Keio University School of Medicine
Yusuke Oguchi
RIKEN Cluster for Pioneering Research
Nobutake Suzuki
The University of Tokyo
Tsuyoshi Kiniwa
RIKEN
Hiroki Kabata
Keio University School of Medicine
Tatsuhiko Tsunoda
The University of Tokyo
Fuyuki Miya
Tokyo Medical and Dental University
Keisuke Goda
University of Tokyo https://orcid.org/0000-0001-6302-6038
Osamu Ohara
Kazusa DNA Research Institute https://orcid.org/0000-0002-3328-9571
Koichi Fukunaga
Keio University School of Medicine
Kazuyo Moro
Osaka University
Sotaro Uemura
The University of Tokyo
Yoshitaka Shirasaki (yoshitaka.shirasaki@bs.s.u-tokyo.ac.jp)
The University of Tokyo https://orcid.org/0000-0002-3808-1630

Article

Keywords: Time-Dependent Cell-State Selection (TDCSS), innate lymphoid cells (ILC2s)

Posted Date: April 8th, 2021

DOI: https://doi.org/10.21203/rs.3.rs-345276/v1

Version of Record: A version of this preprint was published at Communications Biology on September 6th, 2023. See the published version at https://doi.org/10.1038/s42003-023-05297-w.

Abstract

Cell fate determination, a fundamental process of life, is controlled through dynamic intracellular molecular networks. However, the low population of cells at the switching period of fate determination has made it technically difficult to analyze the transcriptome of the stage. Here we developed the Time-Dependent Cell-State Selection (TDCSS) technique, which detects an index of the switching period by live-cell imaging of secretion activity followed by simultaneous recoveries of the indexed cells for subsequent transcriptome analysis. Specifically, we used the TDCSS technique to study the switching period of group2 innate lymphoid cells (ILC2s) activation indexed by interleukin (IL)-13 secretion onset. TDCSS newly classified time-dependent genes, including transiently induced genes (TIGs). The finding of IL4 and MIR155HG as TIGs demonstrated their regulatory function of ILC2s activation.

Main

Cells decide their fates, such as differentiation[1], cell death[2], stress response[3], and immune response[4,5], through dynamic intracellular molecular mechanisms[6,7]. To understand how cells determine their fate, we need to identify the molecular signatures of the early period of the fate determination process that turns on and off the gene expressions and determine the cell fate (Fig. 1a). In general, because the fate determination is asynchronous[8–10] (Fig. 1b), a cell population collected by “snap-shot” manner at a particular time point contains cells in various stages in the fate determination process (Fig. 1c, d)..

There are two conventional approaches to study cell fate determination processes. Single-cell transcriptome analysis enables us to computationally infer their fate determination process by ordering cells based on similarities in their gene expression patterns[11,12](Fig. 1d). This approach is effective for a slow fate determination process, such as differentiation, but it is not effective for a rapid fate determination process with a short switching period such as inflammation. Further, this approach sometimes incorrectly estimates the cell fate trajectory because of the scarcity of the cells in a switching period among a collected cell population (Fig. 1d). This scarcity is caused not only by the low frequency of cells entering in a switching period but also by the short duration of the period itself [13–15].

Another approach is a longitudinal analysis, such as live-cell imaging (LCI) techniques, that can reliably capture a switching period even if it is infrequent and short by visualizing the molecules associated with the fate determination process[2,10,13,16,17]. However, the LCI analysis misses a broader view of potential factors due to its predetermined molecular dynamics.

Here we report the development of the Time-Dependent Cell-State Selection (TDCSS) technique that combine advantages of LCI and single-cell transcriptome analyses (Fig. 1e). TDCSS is a time-dependent cell recovering method according to the longitudinal cellular state information recorded using an LCI technique that enables the identification of the molecular signatures at the targeted switching period of the fate determination process (Fig. 1c, f) instead of relying on the computational inference for time-dependent analysis. We demonstrate the effectiveness of the TDCSS technique by applying it to mouse

group 2 innate lymphoid cells (mILC2s)[18,19] that select their fate through inducing a rapid type 2 immune response, which produces a tremendous amount of type 2 cytokines. We further demonstrate the power of the TDCSS technique by applying it to the rare human ILC2s (hILC2s) [20–22]and obtained the signature of expression in the switching period of the fate determination process.

Results

Development of the TDCSS Technique

The key technical challenge of our method is integrating the destructive single-cell transcriptome analysis and the non-invasive LCI without compromising the benefits of either one (Fig. 1g). To overcome this challenge, we designed and developed the TDCSS technique to create an index of a switching period using real-time image analysis of LCI and to synchronously harvest the indexed cells for subsequent transcriptome analysis. The TDCSS technique consists of four steps (Fig. 1g): (1) measurements of an individual cell activity using LCI, (2) real-time analyses of the activity trace, (3) decisions of recovery, and (4) recoveries of the target cells. In the measurement step, an image of a cell is acquired using the LCI technique. The acquired image is then analysed in real-time in the analysis step and indexed for a targeted activity of the cell, which results in the third step that determines whether to recover the cell or to abandon that cell and revert to the step 1 for a different cell. In the recovery step, the flagged cell is harvested for transcriptome analysis.

Evaluating the effectiveness of the TDCSS

As a proof of concept and to evaluate the effectiveness of the TDCSS technique, we selected the cytokine secretion response of mILC2 because of the following reasons. First, mILC2 rapidly produces a large amount of type 2 cytokine, such as interleukin (IL)-5 and IL-13, in the activation process[23]. Therefore, the initiation of the switching period is easily detectable by the LCI technique. Second, mILC2 is activated by a humoral factor, such as IL-33[18]. Therefore, the activation response of mILC2 is easily mimicked on microscopy. Third, mILC2s are non-adherent cells, the flagged mILC2s thus can be easily harvested using a glass capillary.

We performed the TDCSS technique as follows. We observed the IL-13 secretion activities of 187 individual ILC2s from mouse fat tissues stimulated by recombinant IL-33 using the real-time single-cell imaging of protein secretion[13] (LCI of secretion activity, LCI-S) (Fig. 2a). The traces of the secretion signal showed that cells started secretion after various latencies over several hours (Fig. 2b). We found that a delay time (Δt) over 0.5 hours from the onset of secretion (index) is needed to reliably flag the target cells (Extended data Fig. 1a).

To validate the TDCSS technique, we compared mRNA levels of *Il13*, which encodes IL-13, between “time-dependent” recovered cells using the TDCSS technique at Δt = 0.5 or 1.0 hours (Extended data Fig. 1b) and “snap-shot” recovered cells only from secretion-positive mILC2s (Fig. 2c) using single-cell quantitative RT-PCR (qRT-PCR) (Fig. 2d). The variation of *Il13* expression of “time-dependent” recovered

mILC2s at ⊿t = 0.5 hours was significantly reduced compared to that of “snap-shot” recovered cells, although the variation in cells at ⊿t = 1.0 hours was larger than the variation in cells at ⊿t = 0.5 hours. These results indicate homogeneity in the *Il13* mRNA level in the switching period of mILC2’s activation process among cells, which diversified within 1.0 hours. In conclusion, we found that using the onset of IL-13 secretion as an index was effective in obtaining the intracellular molecular information of mILC2 in the switching period using the TDCSS technique.

The transcriptome of mILC2 in the switching period

In order to explore the activation process of the mILC2 comprehensively, mILC2s in the switching period (⊿t = 0.5, 1.0, and 1.5 hours) and in others (pre-stimulation, post-activation, and silent; see Methods) were subjected to single-cell RNA-seq (scRNA-seq). Based on the principal component analysis (PCA) or the trajectory inference (TI) results, the switching period cells was found in a cluster/branch different from that of pre-stimulation cells or post-activation cells (Extended data Fig. 2a, b). This indicates that mILC2 has a characteristic gene expression pattern in its switching period of the activation process.

To classify genes expressed in the switching period, we clustered genes with differential expression (DEG) between states (one-way ANOVA $p < 0.05$). In the end, we classified 1,511 DEGs based on the transition modes in their expression levels into six groups: Early induced, Early reduced, Late induced, Late reduced, Transiently reduced, and Transiently induced (Fig. 3a). The results revealed that a large number of genes were dynamically regulated in the switching period of the mILC2’s activation process. Most importantly, the transiently induced genes (TIGs) could only be identified using the TDCSS technique because their expression levels were indistinguishable between pre-stimulation and late stages (Fig. 3b, arrows, the number of DEG was nine between Pre-Stim and Post-activation and was three between Pre-Stim and Silent among 212 genes). The TIGs were composed of genes that were distinct from those induced in the late stage of activation (Fig. 3c). Remarkably, *Mir155hg*, which is the host gene of miR-155 known to be a critical regulator of mILC2 immune response[24,25], was among TIGs (Supplementary table 1, 2). To study TIGs’ functions, we performed gene ontology (GO) analysis and found the relationships with immune activation related terms such as response to peptide and inflammatory response (Fig. 3d). The result that TIG had a uniquely enriched ontology cluster indicates that the TDCSS technique succeeded in revealing the context of the switching period of mILC2’s activation process previously unavailable.

In order to investigate whether the supervision of cellular function related to TIGs was affected by choice of the index, we reassigned the index to the onset of IL-5 secretion and re-identified the TIGs (Extended data Fig. 4a, b). Although some GO terms were shared between IL-5 indexed TIGs and IL-13 indexed TIGs, these two groups of TIGs were not the same (Extended data Fig. 4c, d). These results demonstrate that the TDCSS technique can be used to comprehensively characterise the gene expression in the switching period of the mILC2 activation process.

Identification of TIGs of human ILC2

Because the efficacy of the TDCSS technique was demonstrated by the experiments using mILC2, we next analysed the expression signature of human ILC2 (hILC2)[21,22,26] during the switching period. Besides being a rare cell type in peripheral blood (50–150/mL)[21], hILC2 starts secretion after various latency over several days (Fig. 5a, Extended data Fig. 5a). The populational rarity and temporal heterogeneity make hILC2 in the switching period hard to be recovered by using a “snap-shot” method (Extended data Fig. 5b), which has been an obstacle for studying the activation mechanism of hILC2.

We applied the TDCSS technique to hILC2 by indexing the onset of IL-13 secretion and harvested the hILC2s in the switching period (⊿t within 3 hours). We compared the transcriptomes among hILC2s in the pre-stimulation, in the post-activation (over three days after stimulation), and in the switching period obtained from three donors. We classified 453 differentially expressed genes into six groups in the same manner described in the mILC2 study (Fig. 4b). We obtained 10 TIGs (*CARD16*, *HPGDS*, *STK17B*, *C9orf135*, *RTKN2*, *FRY*, *CS*, *STAT4*, *MIR155HG* and *IL4*) (Fig. 4c). Remarkably, TIGs of hILC2s also included *MIR155HG*, same as those of mILC2s, and *IL4* which encodes IL-4. IL-4 is a key inducer of type 2 immune response[27] and has an important role in the hILC2 function, including proliferation and maintaining of the CRTh2 expression[28]. Although hILC2 has been thought as a source of IL-4[20], it was difficult to characterize the IL-4 secretion dynamics of hILC2 due to its low production of IL-4. Therefore, we examined IL-4 secretion dynamics from individual hILC2s by LCI-S and confirmed their transient secretion for several hours (Fig. 4d).

Discussion

We succeeded in a holistic exploration of the potential regulators of the fate determination by developing and using the TDCSS technique to harvest individual cells at the switching period even though such potential regulators existed in a small population of cells and only for a short duration. Discovering a uniquely enriched gene ontology cluster of the transiently induced genes (Fig. 3d) indicates that the TDCSS technique is able to exploit the IL-13 secretion onset to identify the characteristic state during the activation process of the ILC2.

The process of how activated ILC2s determine their fate to produce tremendous amount of cytokine[18,29] was unknown. *IL4* and *MIR155HG*, whose respective products IL-4 and miR-155 are two positive regulators of the cytokine production and proliferation of the ILC2[24,28], are upregulated in the switching period of the activation process, suggesting that they are key regulators of the following activation process. MiR-155 is known to target and repress IL-33 signalling repressors, including *INPP5D*[29–31] and *DUSP10*[32,33]. Although these genes were not expressed immediately after the secretion onset of the IL-13, they were expressed at the late stage of the activation process under the IL-33 stimulation (Extended data Fig. 5g). *MIR155HG* might be prepared to silence these negative regulators from the switching period of the activation process to maintain ILC2s’ proliferation and their cytokine production activity. Furthermore, miR-155 also targets *SOCS1*[34,35] and *DUSP4*[36,37], both encoding inhibitors of IL-2 signalling that support ILC2’s activation[38,39], and *IFNGR1*[40], encoding a receptor of IFN-g that suppresses ILC2’s activation[41].

This indicates that miR-155 contributes to the fate determination in several ways. IL-4[28], the other positive regulator we focused on, was confirmed to be transiently produced at the protein level. Our data show a constant expression of *IL4R*, which encodes an IL-4 receptor. This implies that IL-4 produced by ILC2 early in its activation contributes to the positive regulation of activation in an autocrine manner though further studies are required to support this. Genes expressed in the switching period of the activation process but currently with unknown function in the ILC2 should be studied in the future in order to better understand the fate determination mechanism of the ILC2.

While we focused on the activation process of ILC2 in this study, many LCI techniques have been developed to trace various fate determination processes, including immune response[16], cell differentiation[42,43], cell death[2], and stimulus response[10,44]. Using these LCI techniques, the TDCSS technique will help elucidating contexts of these fate determination processes as well. The gene expression analysis using the TDCSS technique has the advantage of being able to robustly investigate the fate determination mechanism at a targeted stage but it is not suitable for understanding the continuous aspect of the entire fate determination process. On the other hand, the computational inference methods allow us to obtain a global perspective of the fate determination process, though it suffers shortcomings from an algorithm-dependency[45]. A combined approach of the TDCSS technique and computational inference methods will robustly define the fate determination process, leading to a comprehensive understanding of the whole picture of the fate determination processes.

Methods

Reagents

For cytokine secretion imaging using the LCI-S, we used anti-human IL-13 (MAB213 and BAF 213) and IL-4 (MAB604 and BAF204), anti-mouse IL-13 (MAB413 and BAF413) and IL-5 (MAB405 and BAM705) antibodies (R&D Systems, Minneapolis, MN, USA). For cell sorting of hILC2s, we used lineage antibody cocktails of human CD3 (UCHT1), CD14 (HCD14), CD16 (3G8), CD19 (HIB19), CD20 (2H7), CD56 (HCD56), PE-conjugated anti-human CD127 (A019D5), PE/Cy7-conjugated anti-human CD161 (HP-3G10) antibodies (BioLegend, San Diego, CA, USA), and Alexa Fluor 647-conjugated anti-human CRTH2 (BM16) antibody (BD Biosciences, San Jose, CA, USA).

For human ILC2 stimulation, we used recombinant human IL-2 (Imunace35, Shionogi & Co., Ltd, Japan), IL-33, and TSLP (3625-IL/CF and 1398-TS/CF, R&D Systems, Minneapolis, MN, USA). For mILC2 stimulation, we used recombinant mouse IL-2 and IL-33 (402-ML and 3626-IL, R&D Systems).

Isolation of human ILC2s

Peripheral blood was obtained from healthy volunteers at Keio University School of Medicine. This study was approved by the Institutional Review Board of Keio University School of Medicine. All subjects provided their written informed consent.

For isolation of ILC2s from human peripheral blood, mononuclear cells were obtained using Lymphoprep™ (Axis-Shield, Dundee, UK), according to the manufacturer's protocols. Lineage-negative (CD3, CD14, CD16, CD19, CD20 and CD56) and CD45-, CD127-, CRTH2- and CD161-positive cells were sorted using a MoFlo™ XDP flow cytometer (Beckman Coulter, Brea, CA, USA).

Preparation of mouse ILC2

We isolated mouse ILC2s from mouse fat tissues using a previously described protocol[1]. Briefly, we obtained pooled mesentery from 20 wildtype C57BL/6 mice. Lineage-negative cells were selected by negative selection using MicroBeads and AutoMACS (Miltenyi Biotec GmbH). Then, c-Kit + Sca-1 + cells were sorted as ILC2s using a FACSAria flow cytometer (BD Bioscience). The acquired mouse ILC2s were cultured for several months in RPMI-1640 media (R8758, Sigma-Aldrich, St. Louis, MO, USA) containing 10% fetal calf serum (FCS) (S1820, Japan Bioserum, Hiroshima, Japan), 10 mM HEPES buffer (H3537, Sigma-Aldrich), 1 mM sodium pyruvate (11360-070, Thermo Fisher Scientific, Waltham, MA, USA), 1x non-essential amino acids (M7145, Sigma-Aldrich), 100 U/mL penicillin and 100 µg/mL streptomycin (15140-122, Thermo Fisher Scientific), 14.3 mM 2-mercaptoethanol (21985023, Thermo Fisher Scientific), and 10 ng/mL recombinant mouse IL-2 (1399-IL, R&D Systems) in 96-well round-bottom plates. ILC2 cells were usually isolated from retired female breeder mice unless stated otherwise. All experiments were approved by the Animal Care and Use Committee of RIKEN or Keio University and performed according to institutional guidelines.

LCI of secretion activity of ILC2s

A fully automated inverted microscope (ECLIPSE Ti-E; Nikon, Tokyo, Japan) was used for time-lapse imaging using total internal reflection fluorescence (TIRF) illumination of LED light (X-Cite XLED1, mounted with RLX: 615–655 nm, Excelitas Technologies Corp., Waltham, MA) through white-light TIRF optics (high-performance Epi-fl illuminator module TI-SFL). The optical configurations used were the following: excitation filter = FF01-635/18; emission filter = FF01-692/40; and dichroic mirror = FF560/659-Di01. These optical filters were purchased from Semrock (Rochester, NY, USA). We introduced pre-stimulation ILC2s into a microfabricated well array dish, which composed with a polydimethylsiloxane (PDMS), amorphous fluorocarbon polymer CYTOP™, and glass with the immobilised capture antibody. We selected wells that contained single cells and immediately started scanning after replacing the medium with detection medium containing CF660R-labeled detection antibody and cytokine stimuli. In the hILC2s experiment, we used a detection medium containing 200 U/mL IL-2, 1 µg/mL IL-33, and 1 µg/mL TSLP. For mILC2s, we used detection medium containing 10 µg/mL IL-2 and 10 µg/mL IL-33. Scan intervals were 15 minutes for hILC2s experiments and 4 minutes for mILC2s experiments.

Detection of the secretion onset

For detection of increased secretion signals from each cell, acquired images were sequentially analysed using Python 3 software developed in-house (https://github.com/TanaYumi/TDCSS). The program calculated the mean intensity of each well and compared the intensity to the first image intensity. The resulting value was used as the secretion signal. When the last three secretion signals were higher than

the value estimated using linear regression of the past signal by one standard deviation, the program notified the operator of potential secretion onset.

After the experiments, we reanalysed the secretion signals to determine the accurate time between secretion onset and cell recovery (⊿t). The secretion onset time was determined by fitting the values to the following formula:

$$signal = \begin{cases} at\ (0 < t < \hat{t}) \\ b(t - \hat{t}) + a\hat{t}\ (\hat{t} \leq t) \end{cases}$$

In the formula, a represents drift, b represents the slope of the secretion signal increase, t represents the time after stimulation and $\hat{t}$ represents the time of secretion onset. The initial value of $\hat{t}$ was set to the visually determined onset on the automated image-analysis system. ⊿t was obtained by calculating the interval between secretion onset and cell recovery.

Cell recovery

Single cells or single colonies were recovered using a glass capillary (L-Tip 15 μm 60° 15 mm, Yodaka Co., Ltd., Kawasaki, Japan) and a pneumatic microinjector (IM-11-2, NARISHIGE, Tokyo, Japan). The glass capillary was positioned using a micromanipulator (TransferMan 4r, Eppendorf, Hamburg, Germany, or Quick Pro, Micro Support Co. Ltd., Shizuoka, Japan). The aspirated cell was ejected to 2.5 μL RNase-free water (06442-95, Nacalai tesque, Kyoto, Japan) for RNA-seq or 2.5 μL of the qRT-PCR reaction mixture (CellsDirect One-Step qRT-PCR Kits, Thermo Fisher Scientific) for qRT-PCR in a PCR tube. The recovered cell was immediately frozen in liquid nitrogen and stored at -80°C until gene expression analysis.

Pre-stimulation cell was recovered before the stimulus addition from the LCI-S platform. In mouse ILC2 experiments, post-activation and silent cell was randomly recovered from cells with positive or negative secretion signal 8 hours after starting the stimulation. In human ILC2 experiments, post-activation and silent cell was randomly recovered 60 hours (2 specimens) or 120 hours (1 specimen) after starting the stimulation.

qRT-PCR

To increase the accuracy of single-cell mRNA quantification, we added the same amount of ERCC Spike-In RNA (622,819 copies per cell) to each sample and used it as a reference. cDNA was synthesised using CellsDirect One-Step qRT-PCR Kits (Thermo Fisher Scientific) using TaqMan probes targeting four genes (*Il13*, *Il5*, *Gapdh* and *Rplp0*) and four spike-in RNA sequences (ID130, ID136, ID131 and ID85). The TaqMan probes used were: *Il13* (Mm.PT.58.31366752), *Il5* (Mm.PT.58.41498972), *Gapdh* (Mm_GAPDH), *Rplp0* (Mm.PT.58.43894205) purchased from IDT Integrated DNA Technologies (Coralville, IA, USA), ID130 (Ac03459943_a1), ID136 (Ac03459946_a1), ID131 (Ac03459944_a1) and ID85(Ac03459923_a1)

purchased from Thermo Fisher Scientific. The PCR product was diluted ten-fold in RNase-free water, and 1 µL of the PCR product was analysed using qPCR using TaqMan Fast Universal PCR Master Mix (Thermo Fisher Scientific). Relative gene expression was calculated using the ΔΔCt method using ID136 as a reference. Samples, where *Gapdh* or *Rplp0* could not be detected, were omitted from the analysis.

RNA sequencing

We synthesised cDNA libraries using SMART-Seq v4 3'-DE Kits (Takara Bio Inc., Shiga, Japan) according to the manufacturer's instructions, with some modifications, adding the synthetic oligo RNA/DNA to suppress undesirable concatemers. A total of 3,892 copies of ERCC spike-in RNA were added to each sample. The cDNA was purified using Agencourt AMPure XP magnetic beads (Beckman Coulter). Library quality check was performed using an Agilent 2100 Bioanalyzer (Agilent Technologies, Santa Clara, CA, USA) and Agilent High Sensitivity DNA Kits (5067-4626). Degraded or low-yield samples were removed. Qubit High Sensitivity assays (Thermo Fisher Scientific) were performed to quantify the cDNA in each library, and 5 or 6 libraries with different indexed primers were evenly pooled. Pooled cDNA (400 pg) was tagmented using Nextera XT DNA Library Prep Kits (Illumina, San Diego, CA, USA), as described in the protocol. Library size and cDNA amount were quantified using an Agilent High Sensitivity DNA Kit and Qubit High Sensitivity assays, respectively. Pooled libraries were sequenced using 91-bp paired-end sequencing on a MiSeq instrument (Illumina). After library demultiplexing and adaptor trimming, we aligned read 1 to reference sequences (human: GRCh38.90, mouse: GRCm38) using TopHat[2], and the read counts were calculated using HTSeq[3].

The normalisation of count data

Acquired read count data were converted to counts per million (CPM) and log2-transformed. Then, log2(CPM+1) values were normalised using the trimmed mean of M values (TMM) method. Genes whose mean log2(CPM+1) value was over ten were used for normalisation.

Principal component analysis

PCA was performed using the Python 3 module "Scikit-learn[4]". We used all genes for the PCA, except for genes with log2(CPM+1) > 1 under 9 cells.

Hierarchical clustering analysis

The hierarchical clustering was performed using the Python 3 module "Seaborn".

Pseudo-time analyses

The pseudo-time analysis was performed using Monocle[6] with default parameters.

K-Means clustering

K-Means clustering was performed with the Python 3 module “Scikit-learn[4]”. In the human ILC2s analysis, mean log2-transformed expression values were calculated among cells in the same state (Fig. 4b).

Enrichment analysis

We used Metascape34 for enrichment analysis using default settings.

Statistical analysis

Variety of the expression levels acquired by qRT-PCR experiment was tested by F-test.

To identify the differentially expressed genes among groups, one-way ANOVA was performed. Genes with $P < 0.01$ (human ILC2) or < 0.05 (mouse ILC2) were classified as highly variable. We used these highly variable genes for subsequent analyses.

Differential expression analysis of LateA vs. PreStim cells and LateA vs. LateS cells was performed using the Mann-Whitney rank test by SciPy 1.0[5] on genes that were expressed in more than four cells and had a fold-change over 3. Genes with a p-value < 0.05 (FDR is calculated under 0.1 using the Benjamini-Hochberg method) were selected as differentially expressed genes.

Declarations

DATA AVAILABILITY AND CODE AVAILABILITY STATEMENT

RNA-sequencing data will be available through the GEO database. Source Data for Figs. –4 and Extended Data Figs. 1–5 are provided with the paper. Other datasets generated during and/or analysed during the current study are available from the corresponding authors on reasonable request.

ACKNOWLEDGEMENTS

The authors would like to thank Mr. Hirotaka Matsumoto, Ms. Kaede Miyata, and Mr. Kazuki Yoda for their scientific advice and Yodaka Co. Ltd (Kawasaki, Japan) for supporting the cell recovery system, and for Mr. Mitsutaka Shirasaki who corrected the English text.

This study was supported by JST PRESTO (grant no. JP17940748 to Y.S.), the Japan Agency for Medical Research and Development (grant no. 10104030), the ImPACT Program of the Council for Science, Technology, and Innovation (Cabinet Office, Government of Japan), JST CREST (JPMJCR 1412 to T.T), the Japan Society for the Promotion of Science (grant no. 18J20143 to Y.T., JP15H01366, JP17H05496 and 20293648 to Y.S., Core-to-Core Program), and White Rock Foundation. This manuscript was edited by Life Science Editors.

AUTHOR CONTRIBUTIONS

Y.T., Y.S. and M.Y. conceived the study and designed the experiments. Y.T., Y.S., M.Y., Y.O. and N.S. established the measurement equipment and environment and the analysis environment. Y.T. and Y.S. performed and analysed the experiments. Y.M., T.K. and K.M. provided the murine sample. T.K. and H.K. prepared the human sample. Y.S., T.T., K.G., O.O., K.F., K.M. and S.U. supervised the experiments. Y.T., Y.S., K.G., O.O., K.F., K.M. and S.U. contributed to acquisition of the financial support for the project leading to this publication. Y.T., Y.S., M.Y., Y.M., T.K, H.K., K.F., K.M. and S.U. interpreted the biological significance of the results. Y.T., Y.S., T.K., Y.O., T.T. and F.M. examined the statistical adequacy of the analysis. Y.T., Y.S. and M.Y. interpreted the data and wrote the paper.

COMPETING INTEREST DECLARATION

The University of Tokyo has filed a patent application covering the methodology of cell recovery system described in this paper. M.Y. has a financial interest in Live Cell Diagnosis, Ltd., the company that was launched for the development of LCI-S. K.G. is a shareholder of CYBO and Cupido.

References

MAIN REFERENCES

1. Tang, F. *et al.* Tracing the derivation of embryonic stem cells from the inner cell mass by single-cell RNA-seq analysis. *Cell Stem Cell* **6**, 468–478 (2010).
2. Liu, T. *et al.* Single-Cell Imaging of Caspase-1 Dynamics Reveals an All-or-None Inflammasome Signaling Response. *Cell Rep.* **8**, 974–982 (2013).
3. Clerk, A. *et al.* Signaling pathways mediating cardiac myocyte gene expression in physiological and stress responses. *J. Cell. Physiol.* **212**, 311–322 (2007).
4. Best, J. A. *et al.* Transcriptional insights into the CD8 + T cell response to infection and memory T cell formation. *Nat. Immunol.* **14**, 404–412 (2013).
5. Amit, I. *et al.* A module of negative feedback regulators defines growth factor signaling. *Nat. Genet.* **39**, 503–512 (2007).
6. Spiller, D. G., Wood, C. D., Rand, D. A. & White, M. R. H. Measurement of single-cell dynamics. *Nature* **465**, 736–745 (2010).
7. Jeknić, S., Kudo, T. & Covert, M. W. Techniques for studying decoding of single cell dynamics. *Frontiers in Immunology* **10**, 755 (2019).
8. Carlo, D. Di & Lee, L. P. Dynamic Single-Cell Analysis for Quantitative Biology. *Anal. Chem.* **78**, 7918–7925 (2006).
9. Polonsky, M., Chain, B. & Friedman, N. Clonal expansion under the microscope: studying lymphocyte activation and differentiation using live-cell imaging. *Immunol. Cell Biol.* **94**, 242–249 (2016).
10. Park, M. C., Hur, J. Y., Cho, H. S., Park, S. H. & Suh, K. Y. High-throughput single-cell quantification using simple microwell-based cell docking and programmable time-course live-cell imaging. *Lab Chip* **11**, 79–86 (2011).

11. Saliba, A. E., Westermann, A. J., Gorski, S. A. & Vogel, J. Single-cell RNA-seq: Advances and future challenges. *Nucleic Acids Research* **42**, 8845–8860 (2014).
12. Klein, A. M. *et al.* Droplet Barcoding for Single-Cell Transcriptomics Applied to Embryonic Stem Cells. *Cell* **161**, 1187–1201 (2015).
13. Shirasaki, Y. *et al.* Real-time single-cell imaging of protein secretion. *Sci. Rep.* **4**, 4736 (2014).
14. Mitrophanov, A. Y. & Groisman, E. A. Positive feedback in cellular control systems. *BioEssays* **30**, 542–555 (2008).
15. Ohno, S. *et al.* Kinetic Trans-omic Analysis Reveals Key Regulatory Mechanisms for Insulin-Regulated Glucose Metabolism in Adipocytes. *iScience* **23**, 101479 (2020).
16. Tay, S. *et al.* Single-cell NF-kappaB dynamics reveal digital activation and analogue information processing. *Nature* **466**, 267–71 (2010).
17. Chyan, W. & Raines, R. T. Enzyme-Activated Fluorogenic Probes for Live-Cell and in Vivo Imaging. *ACS Chemical Biology* **13**, 1810–1823 (2018).
18. Moro, K. *et al.* Innate production of TH 2 cytokines by adipose tissue-associated c-Kit+ Sca-1+ lymphoid cells. *Nature* **463**, 540–544 (2010).
19. Neill, D. R. *et al.* Nuocytes represent a new innate effector leukocyte that mediates type-2 immunity. *Nature* **464**, 1367–1370 (2010).
20. Camelo, A. *et al.* IL-33, IL-25, and TSLP induce a distinct phenotypic and activation profile in human type 2 innate lymphoid cells. *Blood Adv.* **1**, 577–589 (2017).
21. Bartemes, K. R., Kephart, G. M., Fox, S. J. & Kita, H. Enhanced innate type 2 immune response in peripheral blood from patients with asthma. *J. Allergy Clin. Immunol.* **134**, 671 (2014).
22. Mjösberg, J. M. *et al.* Human IL-25-and IL-33-responsive type 2 innate lymphoid cells are defined by expression of CRTH2 and CD161. *Nat. Immunol.* **12**, 1055–1062 (2011).
23. Arner, E. *et al.* Transcribed enhancers lead waves of coordinated transcription in transitioning mammalian cells. *Science (80-.).* **347**, 1010–1014 (2015).
24. Johansson, K., Malmhäll, C., Ramos-Ramírez, P. & Rådinger, M. MicroRNA-155 is a critical regulator of type 2 innate lymphoid cells and IL-33 signaling in experimental models of allergic airway inflammation. *J. Allergy Clin. Immunol.* **139**, 1007-1016.e9 (2017).
25. Knolle, M. D. *et al.* MicroRNA-155 Protects Group 2 Innate Lymphoid Cells From Apoptosis to Promote Type-2 Immunity. *Front. Immunol.* **9**, 2232 (2018).
26. Lim, A. I. *et al.* IL-12 drives functional plasticity of human group 2 innate lymphoid cells. *J. Exp. Med.* **213**, 569–583 (2016).
27. Fallon, P. G. *et al.* IL-4 induces characteristic Th2 responses even in the combined absence of IL-5, IL-9, and IL-13. *Immunity* **17**, 7–17 (2002).
28. Bal, S. M. *et al.* IL-1β, IL-4 and IL-12 control the fate of group 2 innate lymphoid cells in human airway inflammation in the lungs. *Nat. Immunol.* **17**, 636–645 (2016).

29. Furusawa, J. *et al.* Critical role of p38 and GATA3 in natural helper cell function. *J. Immunol.* **191**, 1818–26 (2013).
30. Petrova, T., Pesic, J., Pardali, K., Gaestel, M. & Arthur, J. S. C. p38 MAPK signalling regulates cytokine production in IL-33 stimulated Type 2 Innate Lymphoid cells. *Sci. Rep.* **10**, 1–15 (2020).
31. O'Connell, R. M., Chaudhuri, A. A., Rao, D. S. & Baltimore, D. Inositol phosphatase SHIP1 is a primary target of miR-155. *Proc. Natl. Acad. Sci. U. S. A.* **106**, 7113–7118 (2009).
32. Yamamoto, T. *et al.* DUSP10 constrains innate IL-33-mediated cytokine production in ST2hi memory-type pathogenic Th2 cells. *Nat. Commun.* **9**, 2–11 (2018).
33. Vlad, G. & Suciu-Foca, N. Induction of antigen-specific human T suppressor cells by membrane and soluble ILT3. *Exp. Mol. Pathol.* **93**, 294–301 (2012).
34. Sporri, B., Kovanen, P. E., Sasaki, A., Yoshimura, A. & Leonard, W. J. JAB/SOCS1/SSI-1 is an interleukin-2-induced inhibitor of IL-2 signaling. *Blood* **97**, 221–226 (2001).
35. Ye, J. *et al.* MiR-155 Regulated Inflammation Response by the SOCS1-STAT3-PDCD4 Axis in Atherogenesis. *Mediators Inflamm.* **2016**, (2016).
36. Huang, C. Y. *et al.* DUSP4 deficiency enhances CD25 expression and CD4 + T-cell proliferation without impeding T-cell development. *Eur. J. Immunol.* **42**, 476–488 (2012).
37. Sandhu, S. K. *et al.* MiR-155 targets histone deacetylase 4 (HDAC4) and impairs transcriptional activity of B-cell lymphoma 6 (BCL6) in the Eμ-miR-155 transgenic mouse model. *Proc. Natl. Acad. Sci. U. S. A.* **109**, 20047–20052 (2012).
38. Roediger, B. *et al.* IL-2 is a critical regulator of group 2 innate lymphoid cell function during pulmonary inflammation. *J. Allergy Clin. Immunol.* **136**, 1653-1663.e7 (2015).
39. Mirchandani, A. S. *et al.* Type 2 Innate Lymphoid Cells Drive CD4 + Th2 Cell Responses . *J. Immunol.* **192**, 2442–2448 (2014).
40. Banerjee, A., Schambach, F., Dejong, C. S., Hammond, S. M. & Reiner, S. L. Micro-RNA-155 inhibits IFN-γ signaling in CD4+ T cells. *Eur. J. Immunol.* **40**, 225–231 (2010).
41. Moro, K. *et al.* Interferon and IL-27 antagonize the function of group 2 innate lymphoid cells and type 2 innate immune responses. *Nat. Immunol.* **17**, 76–86 (2016).
42. Wang, W. *et al.* Live-cell imaging and analysis reveal cell phenotypic transition dynamics inherently missing in snapshot data. *Sci. Adv.* **6**, eaba9319 (2020).
43. Nishimura, K. *et al.* Live-cell imaging of subcellular structures for quantitative evaluation of pluripotent stem cells. *Sci. Rep.* **9**, 1–15 (2019).
44. Davey, A. M., Liu, W., Sohn, H. W., Brzostowski, J. & Pierce, S. K. Understanding the initiation of B cell signaling through live cell imaging. in *Methods in Enzymology* **506**, 265–290 (Academic Press Inc., 2012).
45. Saelens, W., Cannoodt, R., Todorov, H. & Saeys, Y. A comparison of single-cell trajectory inference methods. *Nat. Biotechnol.* **37**, 547–554 (2019).

METHODS REFERENCES

1. Moro, K., Ealey, K. N., Kabata, H. & Koyasu, S. Isolation and analysis of group 2 innate lymphoid cells in mice. *Nat. Protoc.* **10**, 792–806 (2015).
2. Kim, D. *et al.* TopHat2: Accurate alignment of transcriptomes in the presence of insertions, deletions and gene fusions. *Genome Biol.* **14**, R36 (2013).
3. Anders, S., Pyl, P. T. & Huber, W. HTSeq-A Python framework to work with high-throughput sequencing data. *Bioinformatics* **31**, 166–169 (2015).
4. Pedregosa FABIANPEDREGOSA, F. *et al. Scikit-learn: Machine Learning in Python Gaël Varoquaux Bertrand Thirion Vincent Dubourg Alexandre Passos PEDREGOSA, VAROQUAUX, GRAMFORT ET AL. Matthieu Perrot*. *Journal of Machine Learning Research* **12**, (2011).
5. Virtanen, P. *et al.* SciPy 1.0–Fundamental Algorithms for Scientific Computing in Python. *Nat. Methods* **17**, 261–272 (2019).
6. Trapnell, C. *et al.* The dynamics and regulators of cell fate decisions are revealed by pseudotemporal ordering of single cells. *Nat. Biotechnol.* **32**, 381–386 (2014).

Figures

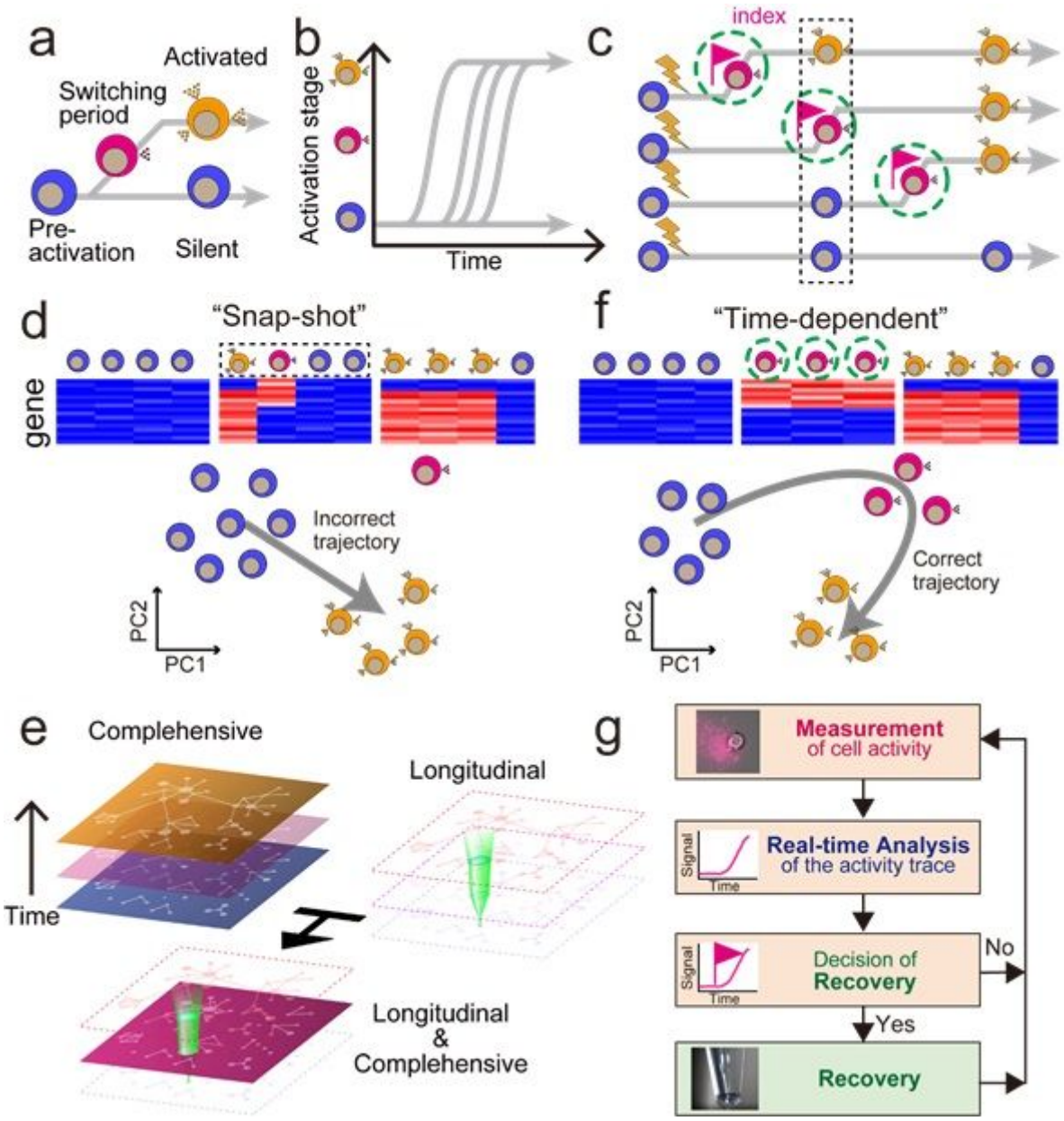

Figure 1

Concept of Time-Dependent Cell-State Selection, TDCSS. (a) Model of cellular state transition during the cell fate determination process. (b)Timings of fate determination are various among cells. (c) Comparison of two cell recovery methods during the cell fate determination process. In the conventional strategy, the cells are collected in a "snap-shot" manner (black rectangle), in spite of collecting in "time-dependent" manner of each cell's transition timing (green circle). (d) The single-cell transcriptomes obtained by the snap-shot cell recovery methods and inferred trajectories of fate determination. (e) The TDCSS technique integrates two techniques. (f) The single-cell transcriptomes obtained by the time-dependent cell recovery methods and inferred trajectories of fate determination. (g) Schematic of the TDCSS technique.

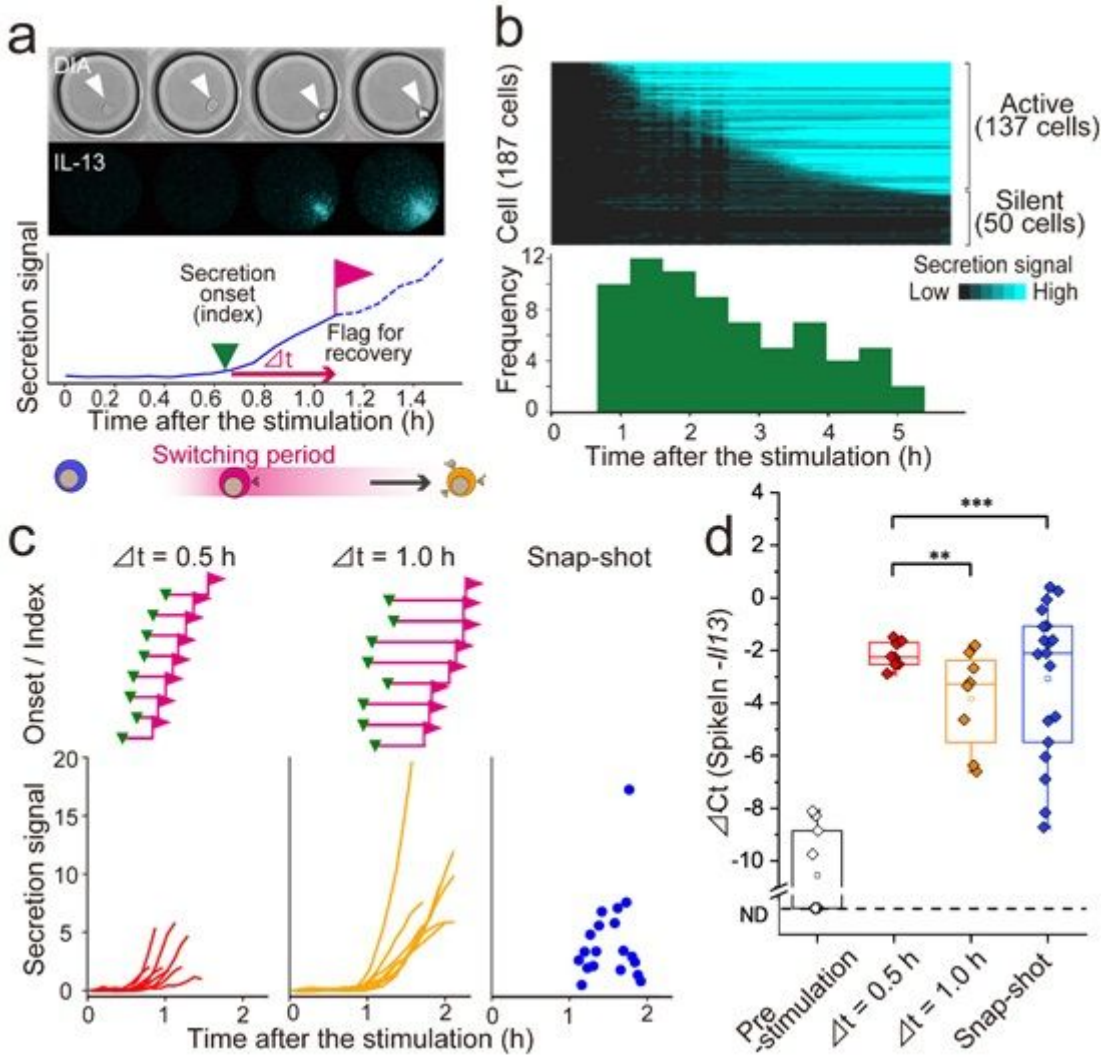

Figure 2

The TDCSS technique found a uniform Il13 mRNA level of mILC2 in switching period. (a) Time-lapse images and intensity trace of IL-13 secretion signal from a stimulated mILC2 acquired by LCI-S. (b) IL-13 secretion signal heatmap of single-mILC2s and a histogram of their secretion onset. (c) IL-13 secretion onset (inverted triangle), recovery timing (flag), and signal trace (bottom) of each mILC2 subjected to qRT-PCR. (d) Box plots show the median and interquartile range of Il13 mRNA levels after the stimulation. Whiskers represent min/max. ND: not detected. **P < 0.01, ***P < 0.001, F-test.

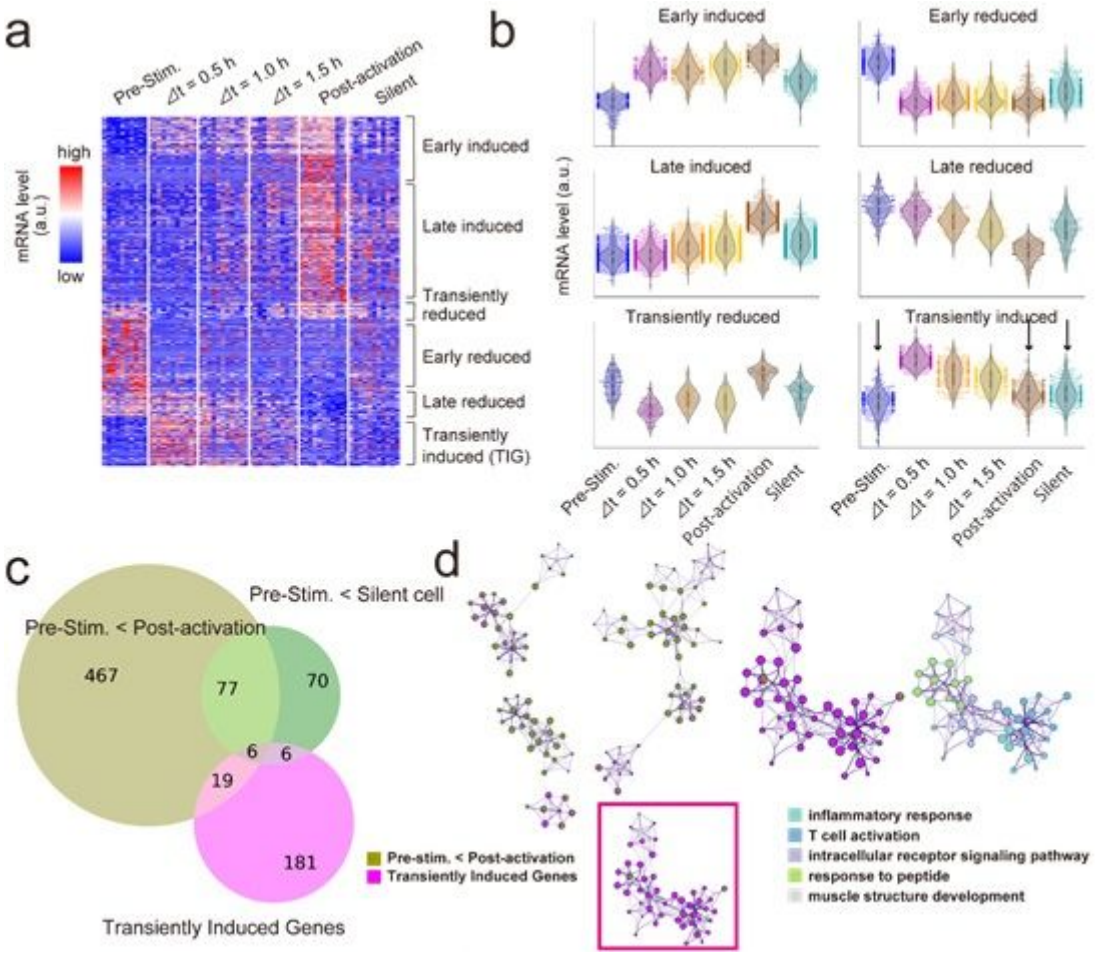

Figure 3

Unbiased characterisation of gene expression during ILC2's activation process. (a) Heat map showing the expression levels of 1,511 DEGs. (b) The expression levels of genes classified into six classes in cells at indicated stages of activation. (c) Overlap of the TIGs with genes upregulated in the post-activation or silent cells compared to the pre-stimulation cells. (d) Enriched ontology clusters of the TIGs and the genes upregulated in the post-activation. The left graph shows the enrichment network in which each node's pie represents the number of genes hit. The right graph shows an enlarged view (left) and clusters coloured by the term (right) of the framed area in the left graph.

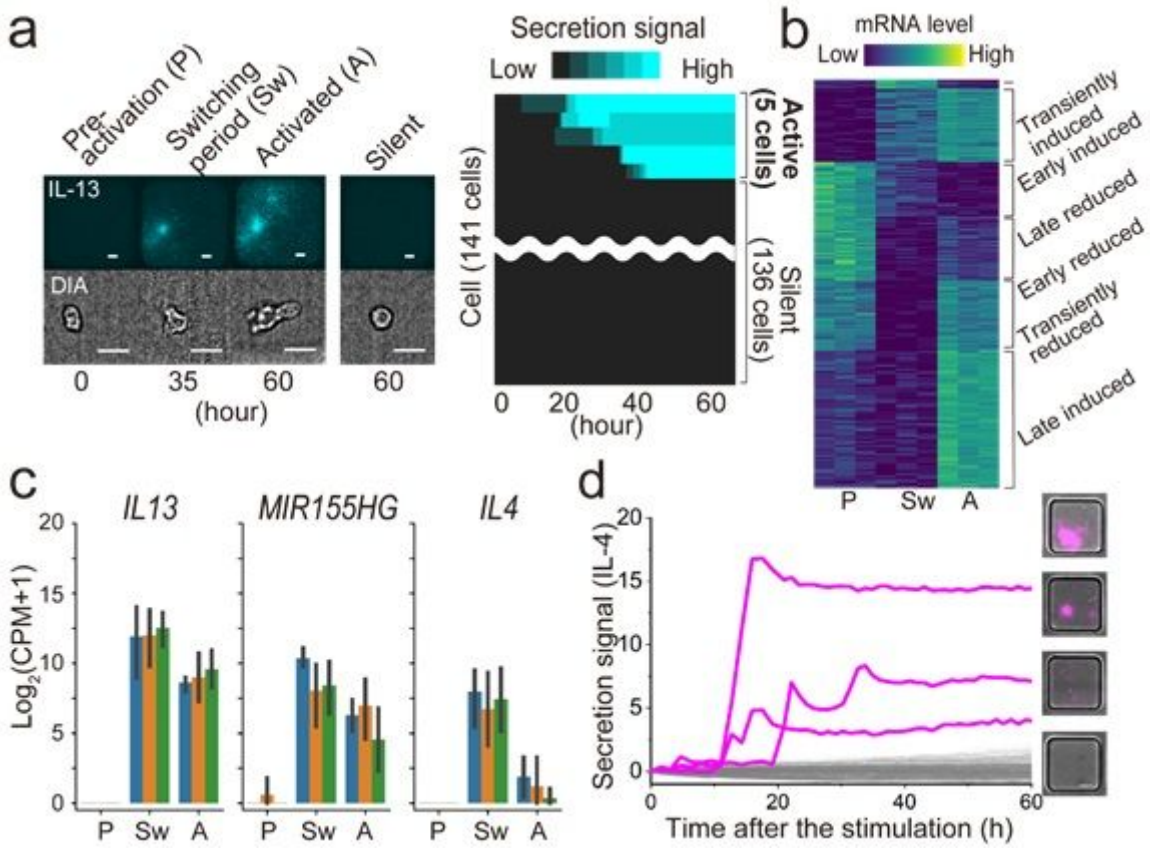

Figure 4

Identification of genes expressed in different activation steps from human specimens. (a) Representative time-lapse images of secretion signal and cell morphology (left) and heatmap of IL-13 secretion signal (right) of single-hILC2s. Scale bar, 25 μm. (b) Heatmap showing mean expression levels of 435 differentially expressed genes. Each column represents a specimen. (c) Expression levels of IL13, IL4 and MIR155HG. Each colour represents a different specimen. Error bars indicate 95% confidence intervals. (d) Secretion signal traces and images of IL-4. Positive secretion traces are shown in magenta.

Supplementary Files

This is a list of supplementary files associated with this preprint. Click to download.

- YumikoTanakaetalNatcommsup.pdf